

Unravelling the origin of the atmospheric moisture deficit that leads to droughts

Received: 11 May 2023

Accepted: 21 December 2023

Published online: 6 February 2024

 Check for updates

Luis Gimeno-Sotelo ¹, Rogert Sorí ¹, Raquel Nieto ¹,
Sergio M. Vicente-Serrano ² & Luis Gimeno ¹ 

Drought is one of the most catastrophic natural hazards, and precipitation plays a major role in the development and intensification of drought events. The amount of precipitation resulting from humidity transported from a given moisture source can be key in revealing the origin of the atmospheric moisture deficit underlying drought occurrence. Here this study demonstrates, for the first time, the predominant role of moisture transport deficit in drought genesis. In most land areas, the estimated conditional probability of drought given an equivalent moisture deficit received either from the ocean or from the continents is higher than 10%. This probability is over 15% in the regions where the main atmospheric moisture transport mechanisms are active and over 20% in some hotspot regions, such as central-east North America, south-east South America and east Europe, where lower incoming moisture is almost synonymous with drought occurrence. Our results indicated that the contribution deficit of the dominant moisture source to the precipitation of a region could improve the predictability of droughts, with enormous hydrological, socioeconomic and environmental implications.

Droughts are the main natural hazard on a planetary scale, responsible for 650,000 deaths from 1970 to 2019¹, billion-dollar economic losses² and ecosystem impacts³. Despite being very complex phenomena that involve several aspects of the hydrological cycle, with several connections to ecosystem processes and water management^{4–8}, the main driving factor of droughts is a precipitation deficit compared with normal conditions^{9,10}. This deficit can essentially occur for three reasons: because there is less moisture available for precipitation, because there is less atmospheric instability that forces air to rise, or a simultaneous occurrence of both. The relationship with moisture content may vary between different locations and seasons depending on the horizontal and temporal scale analysed, with the importance of instability usually being greater than the importance of moisture content, with the exception of its influence on extreme precipitation^{11,12}, where the humidity content is more important than instability. This is why, traditionally, there have been studies on meteorological and climatic conditions that do not favour instability mechanisms and therefore favour the occurrence of droughts (for example, Trenberth et al.¹³).

One major reason for the lower influence of the moisture content than the instability is the fact that it is not possible to determine how much water vapour is involved in precipitation simply from the amount of water vapour in an air column at any given time. The local humidity existing in an air column is mostly insufficient for generating precipitation¹⁴, and lower humidity levels available for precipitation (local and advected) generally imply a deficit in the moisture that reaches the site in question. Therefore, moisture transport deficits generally lead to drought occurrence¹⁵. In this Article, this physical dependence between moisture transport and precipitation is the baseline for studying the statistical relationships between droughts and moisture source contribution deficits.

Atmospheric humidity that causes precipitation in a region can have two origins: (1) direct transport from the ocean or (2) subsequent recycling from the continents themselves^{16–18}. The processes that control evaporation over oceans or continents and moisture transport are very different; additionally, there is a variable relationship between the oceanic and terrestrial origins of precipitation, both globally and

¹Centro de Investigación Mariña, Environmental Physics Laboratory, Universidade de Vigo, Ourense, Spain. ²Instituto Pirenaico de Ecología, Consejo Superior de Investigaciones Científicas, Zaragoza, Spain. ✉e-mail: lgimeno@uvigo.es

regionally¹⁹. The main sources of humidity are those regions where evaporation greatly exceeds precipitation, which mainly occurs in subtropical oceans, some quasi-inland seas (Mediterranean and Red seas), and the two terrestrial areas known as green oceans—the Amazon and Congo river basins²⁰.

The locations where the humidity coming from the entire ocean or continent precipitates have been previously reported¹⁹, as well as the sinks of the humidity that originates from these large individual sources²⁰. The effects of anomalous moisture transport on droughts in specific regions (for example, Drumond et al.²¹)—even in those that are very remote from moisture sources—have also been studied²², as well as the effect of variables closely related to the balance of evaporation and precipitation such as the sea surface salinity (for example, Rathore et al.²³). However, the probability of drought occurrence under a given deficit in moisture transported from global oceanic and terrestrial areas and each of these major sources has not been fully evaluated globally. Understanding the relationship between drought and moisture deficit propagation in the atmosphere would provide a window of opportunity to predict precipitation deficits that has not been explored yet. Lagrangian approaches^{19,24} that analyse moisture transport are highly promising for assessing this issue because they may estimate how much precipitation can be attributed to moisture arriving from a source and reveal the origin of the atmospheric moisture deficit underlying the occurrence of droughts. Applying this approach, we have quantified the extent to which moisture transport affects droughts on a global scale, considering both the entire oceanic and terrestrial areas as moisture sources as well as the major individual sources on the planet. Moreover, we have found that, in some world regions, the contribution deficit of the dominant moisture source may have predictive potential for drought occurrence.

Moisture deficit from ocean versus land triggering droughts

Using monthly values of precipitation and moisture source contributions to precipitation from a given source region, we apply techniques from copula theory to estimate the conditional probability of drought occurrence given an equivalent moisture source contribution deficit, that is, using the same threshold in standardized units for the definition of both phenomena (see Methods for details). A moisture source contribution deficit refers to a deficit of the moisture in the sink region as a consequence of a moisture transport deficit from a given source, understood as a transport of humidity from a given source to a given sink of a lower value than the usual (climatological). The moisture source contributions were estimated by Lagrangian techniques on the basis of tracking the positions and changes of specific humidity of all the particles that reach a given grid element and is in line with a set of different methodologies with similar Lagrangian foundations, very successfully used in the last two decades (for example, Stohl and James²⁵, van der Ent et al.¹⁷, Tuinenburg et al.²⁶ and Dey et al.²⁷).

If we account for the contribution of the whole oceanic global area and the whole terrestrial global area, we find that the conditional probability of drought occurrence given a moisture deficit from oceanic or terrestrial origin can be substantially different (Fig. 1 and Supplementary Figs. 1 and 2). It can reach values over two ($P \times 2$), three ($P \times 3$), four ($P \times 4$) or five ($P \times 5$) times greater than 5%, which is the conditional probability that indicates that drought occurrence and moisture transport deficit are independent, meaning that in that situation a moisture source contribution deficit does not have any influence on drought occurrence. Figure 1 is the representation of those spatial patterns ($P \times 2$, $P \times 3$, $P \times 4$ and $P \times 5$), which show the regions where a moisture deficit from oceanic or terrestrial origin is strongly associated with drought occurrence on an annual scale.

The $P \times 2$ pattern is very similar to that of the percentage contribution to precipitation of oceanic and terrestrial origins (see Fig. 2c in Gimeno et al.¹⁹). Regions where the oceanic origin of precipitation is

dominant experience higher drought probabilities given a moisture contribution deficit from the global oceanic area (Fig. 1a,c); similarly, in regions where the terrestrial component dominates, moisture contribution deficits from the global terrestrial area lead to higher drought probabilities (Fig. 1b,d). When analysing the terrestrial origin of precipitation, it is observed that the continental area where drought occurrence is influenced by the moisture deficit from terrestrial origin is very large, including almost the whole Eurasian continent, America and a large part of Africa and Australia. This highlights the importance of recycling processes in drought occurrence²⁸ given the high level of land evapotranspiration in continental regions^{29,30}. The spatial pattern is very similar, regardless of whether drought is defined with monthly or seasonal Standardized Precipitation Index (SPII or SPI3, respectively) values. Moreover, a similar spatial pattern between time scales can also be identified when the threshold is changed according to the higher probabilities $P \times 3$, $P \times 4$ and $P \times 5$.

As the conditional probability of drought increases ($P \times 3$ and $P \times 4$), the areas become more restricted, and the patterns reveal the regions where the main activity of moisture transport mechanisms takes place at a planetary scale^{15,31}. For instance, the role of atmospheric rivers (ARs) in the oceanic origin of drought can be observed in areas in which precipitation is dominated by this phenomenon (for example, western coasts of North America and Europe)³². Moreover, the roles of tropical cyclones (TCs) in the oceanic origin of drought (for example, the eastern coast of North America) and that of low-level jets (LLJs) in the oceanic origin of drought in northern South America or in the terrestrial origin in the La Plata basin, whose main moisture source is the Amazon basin, are visible^{33,34}. In regions with no major moisture transport mechanisms, such as the interior of the Eurasian continent, the influence of recycling and propagation between terrestrial sources and sinks has been observed in drought development³⁵. Terrestrial evapotranspiration changes are expected as a consequence of anthropogenic forcing³⁶. Further, key variations in the position and intensity of moisture transport mechanisms, including an increase in the intensity and poleward displacement of ARs³⁷, changes in the frequency, intensity and position of some LLJs³⁸ and a reduction in the frequency of TCs³⁹ is also expected. These changes have implications for the future occurrence and intensity of droughts in the regions indicated by $P \times 3$ and $P \times 4$.

There are some hotspot regions where the conditional probability of drought occurrence, given an equivalent deficit in moisture transported from oceanic or terrestrial sources, is considerably high, with values in the $P \times 5$ category. Considering a SPI at a time scale of 1 month, these areas can be identified in the Pacific and Atlantic coasts of North America, Western Europe and south-eastern China, with a moisture deficit of oceanic origin, and the interior of Eurasia and La Plata basin in South America when the origin is terrestrial. When the drought time scale is increased to 3 months, for the moisture deficit of terrestrial origin, the hotspot regions also include the north American Great Plains and some areas of inner China, southern Africa and Australia.

This influence of the oceanic or terrestrial origin of moisture on the genesis of droughts can be altered by changes in the atmospheric general circulation. Since a global estimate is difficult to achieve with the methodology used in this work, we can get closer to knowing if these are very relevant by quantifying the changes associated with two modes of climate variability that generate important changes in global circulation, namely the El Niño/Southern Oscillation, due to its global effect, and the North Atlantic Oscillation for its regional effects in the North Atlantic. The obtained patterns for the different mode phases (Supplementary Figs. 3 and 4) are not very different except for some slight displacements of the regions where the highest probability values occur and some intensifications of the probabilities in known regions of influence of these modes on precipitation occurrence^{40,41}. As such, a greater extent of the importance of both oceanic and terrestrial sources in the genesis of drought is generally observed for the negative

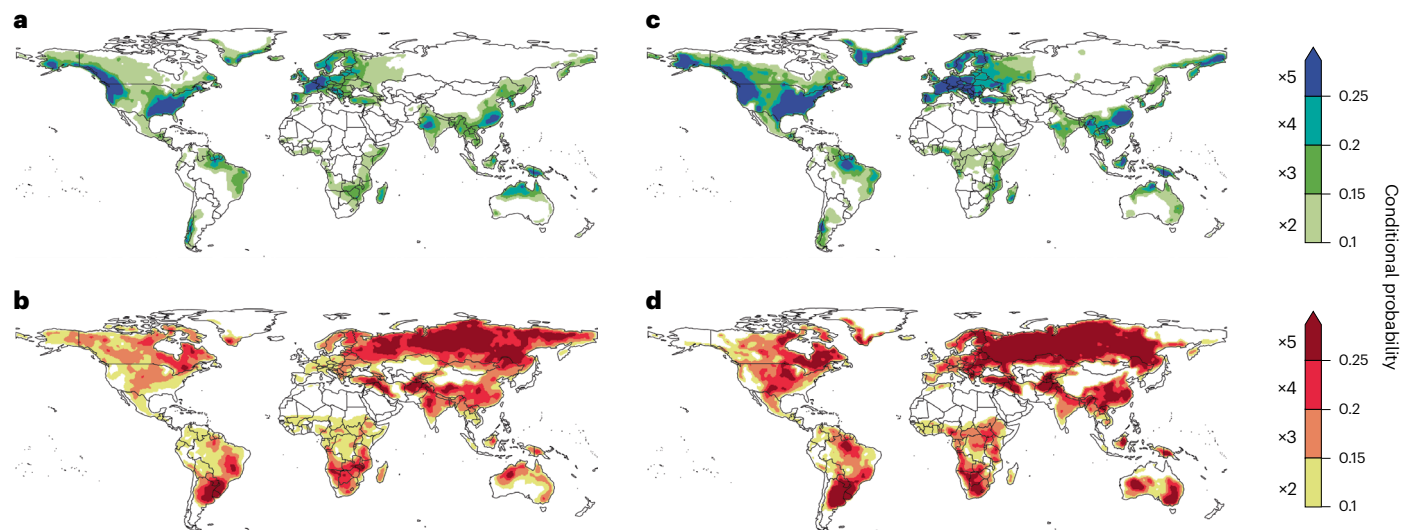


Fig. 1 | Conditional probability of drought occurrence given an equivalent moisture deficit from oceanic or terrestrial origin on an annual scale. **a–d**, Moisture deficit from oceanic origin for SPI time scales of 1 month (**a**) and 3 months (**c**) and from terrestrial origin for SPI time scales of 1 month (**b**) and 3 months (**d**). Probability is expressed as how many times greater it is than that of

the independence case (5%), together with the corresponding values. Statistical method I was applied to the contribution to precipitation of oceanic and terrestrial origins (see Methods for details). A Gaussian filter was used to remove the spatial random noise (original values can be found in Supplementary Figs. 1a,d and 2a,d).

phase of El Niño/Southern Oscillation in comparison with the positive one, and of the oceanic source in the positive phase of North Atlantic Oscillation compared with the negative one.

Moisture deficit from major sources leading to droughts

Once the oceanic or terrestrial origin of the moisture deficit that generates drought is revealed, it is also possible to know the major planetary moisture source responsible for this deficit. Considering the conditional probability of drought given an equivalent moisture deficit from the major planetary moisture sources on an annual scale (Fig. 2), the spatial pattern of the regions where each moisture source is most influential in terms of droughts is similar to that regarding precipitation occurrence (see Fig. 4 in Gimeno et al.²⁰) and extreme precipitation (see Fig. 5a in Vázquez et al.²⁴). A detailed analysis of the conditional probability of drought given a deficit from each of these major moisture sources shows noticeable spatial differences and well-delineated regions of influence, as well as some seasonal differences mainly evidenced in the extension of the sinks (Supplementary Figs. 5–17).

Overall, there is a good match between relevant continental areas identified in Figs. 1 and 2, with the main discrepancies observed in southern Africa and large sectors of Asia. That is so because Fig. 1 accounts for the whole oceanic source and the whole terrestrial source, whereas Fig. 2 only accounts for major oceanic sources and the two major terrestrial ones, the Amazon and Congo basins. It does not include other minor oceanic sources and all terrestrial sources except for the two major ones, which implies the non-inclusion of recycling in all regions with the exception of the Amazon and Congo basins. The North Pacific source has the greatest influence on drought occurrence in the western half of North America and the eastern Asian coast, the Caribbean and Gulf of Mexico sources in the eastern half of North America, the North Atlantic source in Western Europe and northeastern South America, the Mediterranean source holds the main influence over the inner Eurasian continent, while the South Pacific and South Atlantic sources hold moderate influence over some coastal regions of South America, South East Asia and Southern Africa. Finally, the Indian sources are the main influence on drought occurrence in continental monsoon regions (Fig. 2). Thus, drought occurrence in most

regions of the Indian subcontinent is mainly influenced by moisture deficits from the northwestern Indian source region; called in these works the Zanzibar Current and Arabian Sea. Additionally, droughts in Australia are mainly affected by a moisture deficit from the central-eastern Indian source. The two terrestrial sources have influence over their own basins and surrounding areas, which are very extended and intense for the Amazon and less extended for the Congo. In general, the extent and magnitude of the influence of the moisture deficit from major moisture sources is greater under a 3 month time scale than under a 1 month time scale.

This general pattern and the probability values could be altered by a very diverse set of factors, such as changes in the extent and position of the sources or changes in the temperature contrast between the continental sink and the oceanic source with variations in the relative humidity in the continental sink. The first of these effects cannot be appreciated in this paper since the methodology used implies the use of the main climatological sources (Methods), but the influence of the second one can be estimated to a certain extent. The land–ocean temperature contrast may play a role since the ocean temperature sets the saturation specific humidity such that it is not able to maintain relative humidity levels when supplying much warmer land (for example, Byrne and O’Gorman⁴² and Wainwright et al.⁴³). For each oceanic moisture source, we have calculated the conditional probability of drought in the continental area where it is dominant, according to Fig. 2a, given an equivalent moisture transport deficit from that source for two subsamples: high land–ocean temperature contrast and low land relative humidity versus low land–ocean temperature contrast and high land relative humidity (Supplementary Table 1). It is expected that, in the case of high temperature contrast between the continental sink and the oceanic source occurring together with low relative humidity in the continental sink, the role of the oceanic source in the precipitation of the land sink decreases. Thus, in that situation, the contribution of moisture from the continental sink region itself by evapotranspiration due to the high evaporative demand would have a greater relevance³⁵, and it can be expected that the probability of drought given a moisture transport deficit from the source will be lower than in the case of low temperature contrast and high relative humidity. Among the 11 oceanic moisture sources considered in this study, the results confirmed what

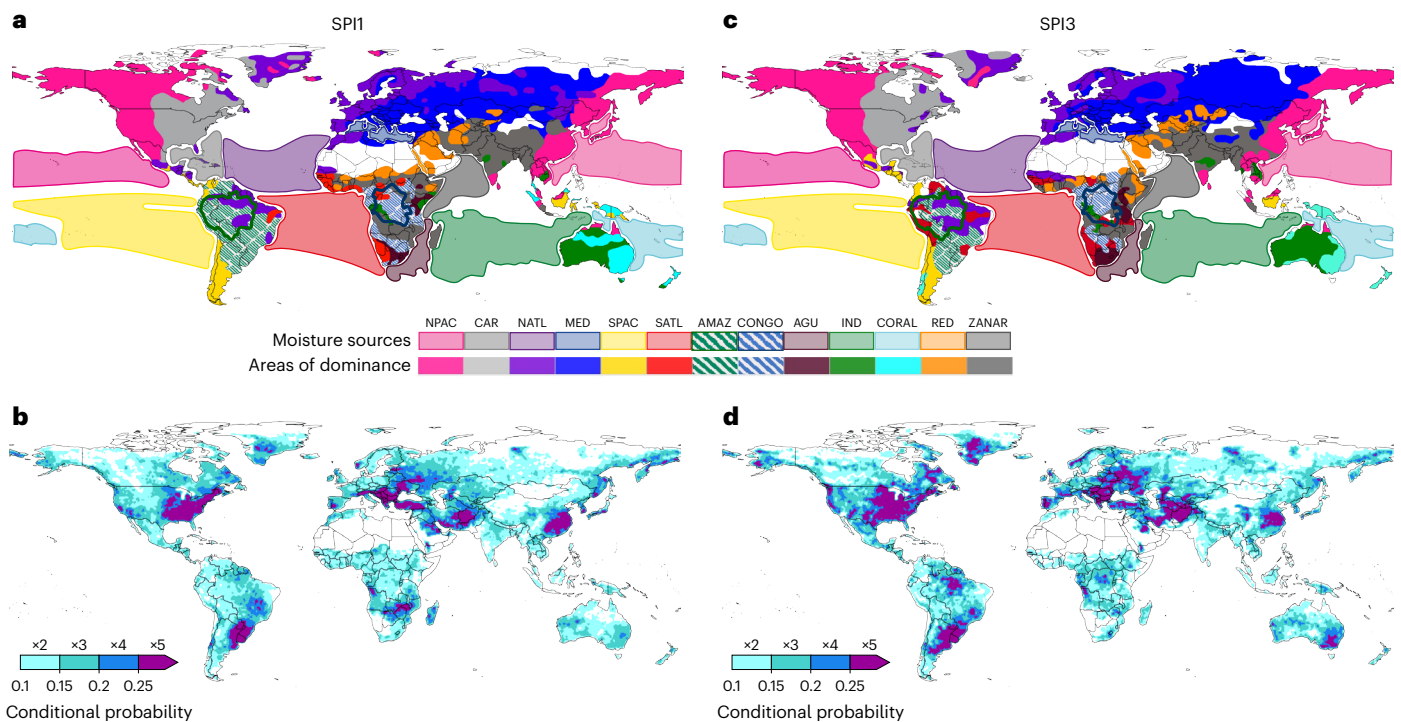


Fig. 2 | Moisture source with the highest associated conditional probability of drought given an equivalent moisture deficit from the major planetary moisture sources (both oceanic and terrestrial), together with the associated probability, on an annual scale. a–d, The spatial pattern of the dominant moisture source for SPI at 1 month (a) and 3 month (c) time scales and the associated probability for SPI at 1 month (b) and 3 month (d) time scales. Probability is expressed as how many times greater it is than that of the independence case (5%), together with the corresponding values. Statistical method I was applied to the contribution to precipitation of each of the major moisture sources (see Methods for details). NPAC, North Pacific Ocean moisture

source; CAR, Caribbean Sea and Gulf of Mexico; NATL, North Atlantic Ocean; MED, Mediterranean Sea; SPAC, South Pacific Ocean; SATL, South Atlantic Ocean; AMAZ, Amazon River basin; CONGO, Congo River basin; AGU, Agulhas Current region; IND, Indian Ocean; CORAL, Coral Sea; RED, Red Sea; ZANAR, Zanzibar Current and Arabian Sea region. Oceanic moisture source regions are coloured with a light shading, and the land areas where each moisture source is dominant are represented by a dark shading. For the Amazon and Congo river basins, they are delimited by solid green and blue lines, and their areas of dominance are represented by oblique lines of those colours, respectively. A Gaussian filter is used to facilitate visualization.

is stated above, finding significant differences in this sense for eight of the sink regions.

Figure 3 focuses on those regions with a high conditional probability ($P \times 3$ and $P \times 4$) of drought occurrence given an equivalent moisture deficit from those major moisture sources on an annual scale. Most areas with $P \times 3$, $P \times 4$ and $P \times 5$ found in Fig. 1 appear, and it is now possible to identify the moisture source regions responsible for the transport deficit. Occasionally, drought occurrence is influenced by the deficit from a single source, such as the North Pacific source for drought conditions in western North America. However, in other cases, multiple sources are responsible, as in the case of eastern North America, with up to three sources influencing droughts in that region: the North Atlantic, North Pacific and Caribbean/Mexican sources. The probability of suffering droughts at time scales of 1 and 3 months when there are deficits in a single moisture source is over four times greater than that of the independence case in three large continental areas (Fig. 3b,d): central-east North America (CENA), associated with a moisture deficit from the Caribbean/Mexican source, south-east South America (SESA), associated with the Amazon source and east Europe (EEur), associated with the Mediterranean source.

Potential of moisture transport in drought predictability

Even with the extraordinary advance of weather and climate models largely linked to the great advance in computing, and better observations and modelling abilities, droughts are very difficult to predict⁴⁴, mainly because of the limited predictability of precipitation over time

spans longer than 15 days⁴⁵. Thus, seasonal to annual precipitation deficit predictions, which are relevant for drought prediction, are highly uncertain, particularly at mid-latitudes^{46,47}. Therefore, and based on the use of models, whether they are weather or climate ones, it could be more advantageous to use predicted moisture transport than predicted precipitation to estimate the predicted occurrence of droughts in the same given future period. The reason for this is that models are able to predict large-scale circulation much better than smaller-scale phenomena, and taking into account that moisture transport is related to larger-scale circulation, it can be assumed that its predictability will be better than in the case of precipitation, which is more conditioned to more complex and smaller-scale atmospheric processes⁴⁸. For medium-range (submonthly) time scales, Lavers et al.⁴⁹ demonstrated that integrated vertical moisture transport (a measure of moisture transport) was more predictable than precipitation in northwestern Europe and the western US, and the results obtained by Gvoždíková and Müller⁵⁰ for Central Europe are in line with it. For seasonal time scales, Wang and Yuan⁵¹ for China's Yangtze River basin and Gao et al.⁵² for the Northern Hemisphere also show the greater predictability of moisture transport. In this study, we show that the moisture transport deficit may affect drought severity in large world regions. Therefore, in regions where moisture transport deficits are strongly related to precipitation deficits, droughts could be potentially predicted on the basis of moisture transport. Figure 4 shows the conditional probability of drought given the observed values of moisture contribution deficits from the main moisture source of each of the three hotspot regions previously discussed, that is, CENA, SESA and EEur. Each of these three

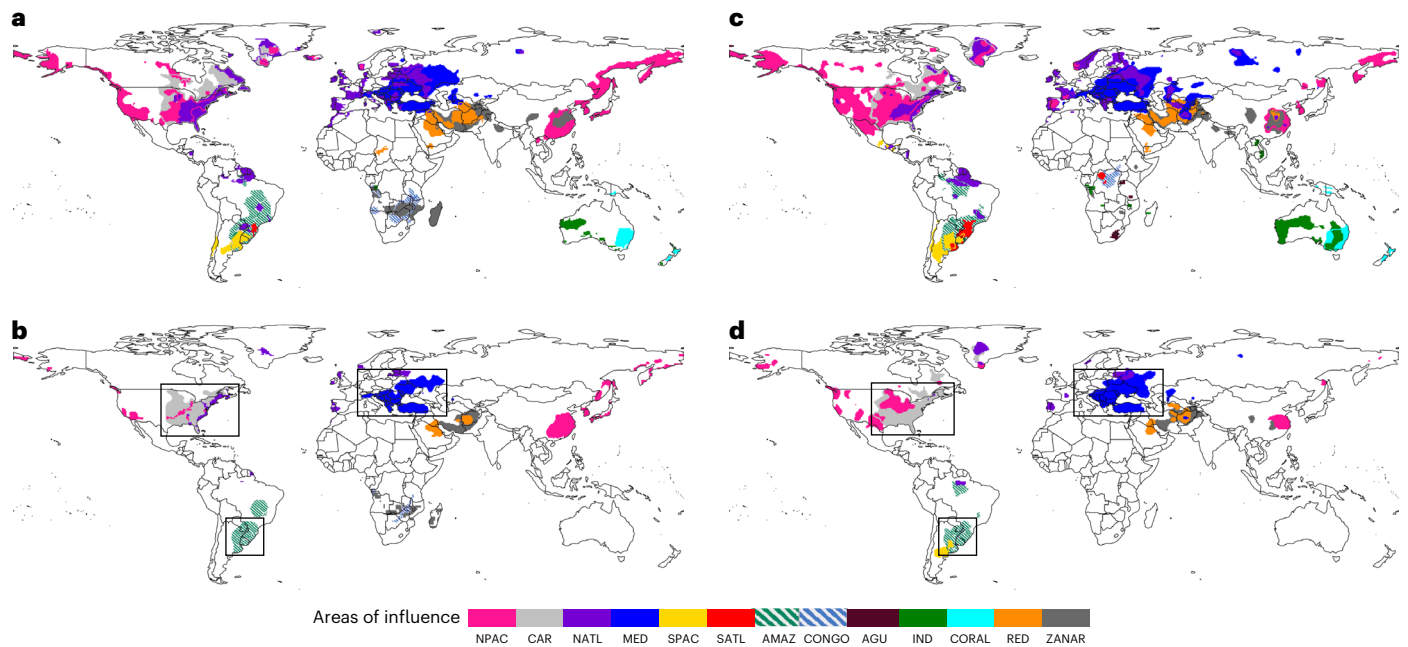


Fig. 3 | Regions where the conditional probability of drought occurrence given an equivalent moisture deficit from the major moisture sources of the planet is over three and four times greater than that of the independence case, respectively, on an annual scale. a–d, Patterns corresponding to a conditional probability over three times (**a** and **c**) or four times (**b** and **d**) greater than the independence case (5%) for SPI at 1 month (**a** and **b**) and 3 month (**c** and **d**) time

scales. In **b** and **d**, the rectangles represent the boundaries of the three large continental areas influenced by a single moisture source with a conditional probability being more than four times greater than the independence case, namely CENA, SESA and EEur. Acronyms of moisture sources are the same as those used in Fig. 2. A Gaussian filter is used to facilitate visualization.

regions have a single dominant major moisture source: the Caribbean/Mexican source for CENA, Amazon source for SESA and Mediterranean source for EEur. Strong moisture source contribution deficits are associated with the highest drought probability values in all regions and time scales. Moreover, the observed cases with the highest values of drought probability corresponded to situations in which extreme and severe droughts took place. This means that the metric generated using moisture source contribution deficits reproduces droughts reasonably well in the analysed regions. Thus, considering a well-known drought event for each of those regions (Supplementary Table 2), the conditional probability of drought given the observed value of the moisture source contribution deficit at the peak of each event was estimated. The peak of the event was determined on the basis of the lowest SPI value. As such, it was found out that the probability of drought was higher than the independence case (5%) for all regions and both the 1 and 3 month SPI. Further, very high probabilities were obtained for CENA using the 1 and 3 month SPI (68.3% and 78.1%, respectively) and for EEur using the 1 month SPI (61.9%).

Conclusions

The results presented demonstrate the key role of the moisture transport deficit in drought genesis, especially in certain regions where drought is caused by a moisture deficit of oceanic or terrestrial origin, and in which drought severity is strongly determined by particular moisture sources. Our results suggest that the conditional probability of drought occurrence is at least two times greater than the independence case (5%) when there is an equivalent deficit of moisture received from either the ocean or continents in most regions. This indicates that moisture deficit plays a notable role in the development and/or intensification of drought events. Moreover, there exist certain hotspot regions in which this probability is three or more times greater than the independence case, owing to their low incoming moisture, as well as other regions in which this probability is much higher (CENA, SESA

and EEur), where a moisture deficit from the major source (Caribbean, Amazon and Mediterranean, respectively) is almost synonymous with drought occurrence.

This work provides an opportunity to improve drought predictability in some world regions. The analysis of the three hotspot regions showed an agreement between the estimated drought probability based on the moisture deficit and the observed drought severity.

Further, this study could be a first step to studying the extent to which global climate change affects the relationship between moisture source contribution deficits and drought occurrence. It is expected that climate change can affect these relationships through shifts in circulation altering the source to sink patterns, mainly associated with changes in position and intensity of the Intertropical Convergence Zone and Hadley cells in tropical regions and the storm track in extratropics^{53,54}. Additionally, these relationships could also be affected by the land–ocean warming contrasts with faster warming over land than the ocean and subsequent continental relative humidity decline, which have implications for current and future changes in moisture supply with impacts on the drought severity and likelihood (for example, Byrne and O’Gorman⁴², Wainwright et al.⁴³ and Allan et al.⁵⁵). In our current climate, this work already points to the direction that the relationship between droughts and moisture transport deficits may be slightly different when there are different conditions of relative humidity and land–ocean temperature contrast or changes in circulation associated with different phases of modes of climate variability.

The seasonal and climatic predictive power of the methodology used in this study opens new relevant topics to be explored, such as the role of the specific moisture sources of a given region in drought development, or the implications for the predictability of flash droughts⁵⁶ or rapid hydrological transitions or ‘whiplash’⁵⁷. These are phenomena that, when developed on smaller time scales than usual droughts, close to the submonthly scale, could benefit from the improved predictability of moisture transport versus precipitation.

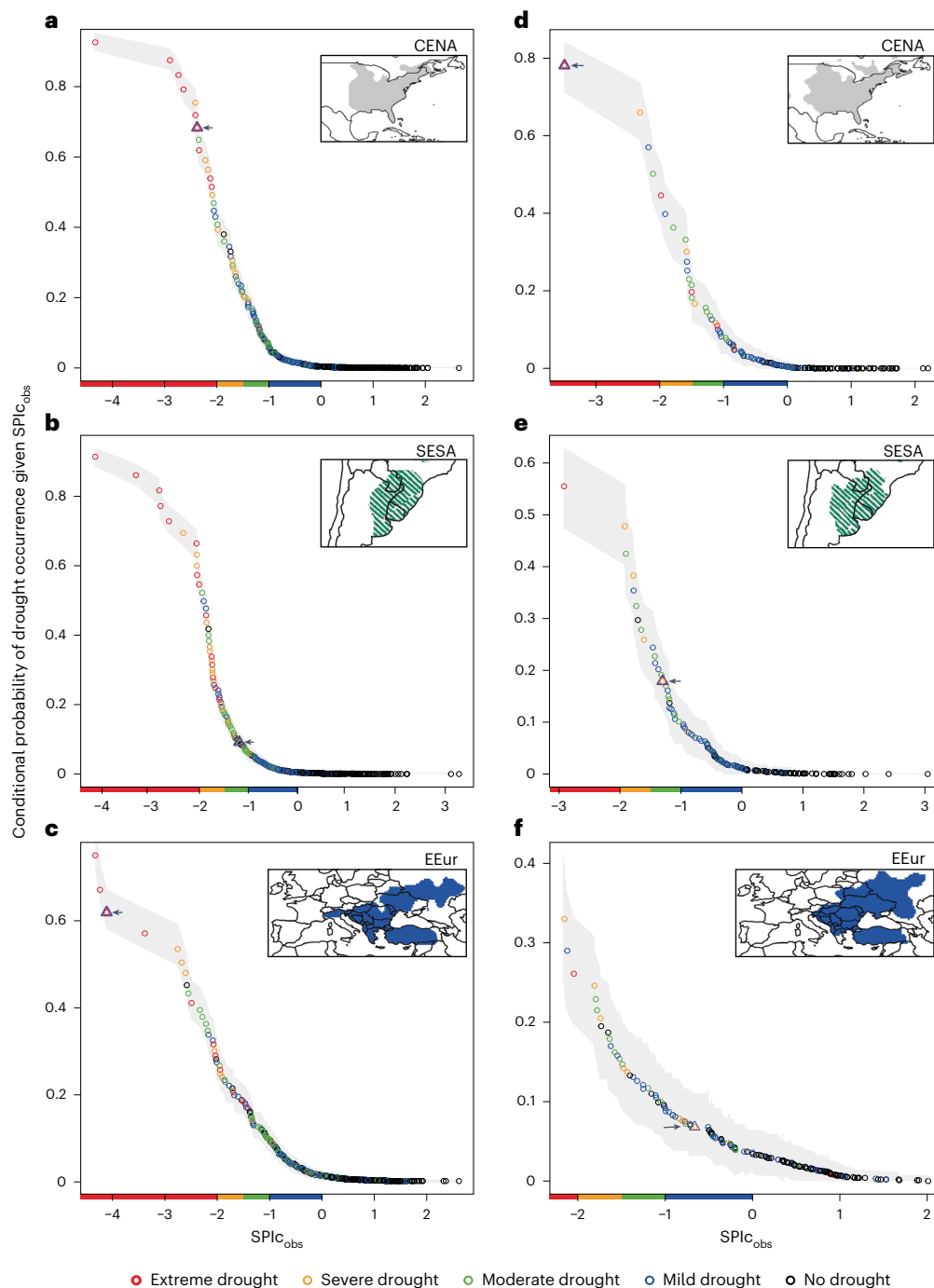


Fig. 4 | Conditional probability of drought occurrence given observed values of moisture contribution deficits from the main moisture source of CENA, SESA and EEur, respectively. a–f. Conditional probabilities for the CENA region using a SPI at the time scales of 1 month (a) and 3 months (d), the SESA region using a SPI at the time scales of 1 month (b) and 3 months (e) and the EEur region using a SPI at the time scales of 1 month (c) and 3 months (f). Statistical method II was applied to the contribution to precipitation series of the Caribbean/Mexican source for CENA, of the Amazon source for SESA and of the Mediterranean source for EEur (see Methods for details). Grey bands indicate 95% statistical

confidence for the conditional probability (measure of centre for the error bands). Drought categories are taken according to the scale defined by McKee et al.⁵⁸, that is, the SPI thresholds of -2 , -1.5 , -1 and 0 refer to extreme droughts (red circles), severe (orange circles), moderate (green circles) and mild ones (blue circles), respectively. For each region and time scale, a purple triangle and an arrow are used to indicate the probability corresponding to the observed value of the moisture source contribution in the peak of the well-known drought event presented in Supplementary Table 2.

Methods

Calculation of drought indices

In this study, droughts were defined as monthly or cumulative precipitation deficits over 1 and 3 month periods obtained using the SPI⁵⁸, denoted as SPI1 and SPI3, respectively. The election of SPI instead of

other indices that include temperature, such as the Standardized Precipitation–Evapotranspiration Index (SPEI)⁵⁹ or the evaporative demand⁶⁰ is twofold: (1) the study focuses on the short-term drought variability. In this case, the role of warming on drought severity is less relevant as the sensitivity of the SPEI to the increased atmospheric evaporative

demand is mostly recorded on long time scales as a consequence of the high autocorrelation that characterises multi-scalar drought indices. Moreover, for the short-term variability, the SPEI is mostly driven by precipitation so the inclusion or not of the atmospheric evaporative demand is not going to produce a large impact on the obtained results, and (2) the study focuses on the role of moisture transport on drought severity so we try to isolate this influence, which is recorded on precipitation. Precipitation is driven by different dynamic and thermodynamic mechanisms but the availability of air moisture is a fundamental driver. On the contrary, the variability of the atmospheric evaporative demand is driven by other mechanisms, fundamentally thermodynamic, including radiative forcing as a consequence of enhanced emissions of greenhouse gases and also land–atmosphere feedbacks associated with the availability of soil moisture and the partition of sensible and latent heat fluxes. Although air humidity is a driver of the vapour pressure deficit, which has a role in the atmospheric evaporative demand, it has been observed that the main driver of changes in atmospheric evaporative demand is temperature. Thus, from a physical perspective, the inclusion of the atmospheric evaporative demand would include some noise in the analysis, as a component that is not expected to be related with air humidity transport would be included. The positive (negative) SPI values represent values that are higher (lower) than the mean precipitation, indicating wet (dry) conditions that can be spatio-temporally compared. Thus, the SPII reflects short-term precipitation conditions and the SPI3 short- and medium-term ones, providing a seasonal estimation of precipitation and reducing the influence of precipitation variability on a monthly scale. The SPI application can be closely related to meteorological types of drought along with short-term soil moisture and crop stress⁶¹, but it is also useful for assessing hydrological and ecological drought impact^{62,63}.

The global gridded SPI was computed using the $0.5^\circ \times 0.5^\circ$ monthly Multi-Source Weighted-Ensemble Precipitation (MSWEP) series for the 1980–2018 period. MSWEP dataset v2.8 (ref. 64) is a high-quality global product that takes advantage over other observed and estimated precipitation datasets because it merges gauge, satellite and re-analysis data. However, it has some limitations in the representation of precipitation in some regions, owing to variations in the number of daily observations and short periods with available data⁶⁴. In some regions, such as Africa, the number of gauge observations is quite low, which might negatively impact the performance of the product, particularly affecting the identification of hydroclimate extremes⁶⁵. Despite this, it has been shown that MSWEP performed better than other rainfall datasets (for example, Integrated Multi-satellite Retrievals for GPM and Climate Hazards Group InfraRed Precipitation with Station data) at the daily time scale over the continent⁶⁶. Another limitation of this product is that the climatology of the precipitation probability distribution in the latest version of MSWEP is based on the European Centre for Medium-Range Weather Forecasts re-analysis ERA5 (ref. 67), which leads to an underestimation of the maximum values, although it can generally capture their locations and patterns⁶⁸.

Calculation of the contribution to precipitation from the whole oceanic and terrestrial moisture sources

The moisture contribution to precipitation over land has two possible origins: the oceans and the continents. Nieto and Gimeno^{69,70} proposed a methodology to obtain both contributions using an approach based on a Lagrangian technique for estimating the precipitation given the moisture transported from the two sources separately, which was already used by Gimeno et al.¹⁹ to study changes in the ratio between them in the current climate. For this study, we used $0.5^\circ \times 0.5^\circ$ monthly datasets for the 1980–2018 period of oceanic and terrestrial moisture contributions to precipitation.

These authors used the outputs of the Lagrangian particle dispersion model FLEXPART v9.0 (refs. 71,72) that moves approximately two million air parcels (of constant mass, m) in which the atmosphere was

divided every 6 h for the period 1980–2018. The air parcels in the model were moved and have the meteorological characteristics given by the ERA-Interim⁷³ re-analysis from the European Centre for Medium-Range Weather Forecasts.

The air parcels residing over the whole ocean and the whole continents, separately, were tracked forwards in time to determine the changes in specific humidity every 6 h (dq/dt , $dt = 6$ h) along each trajectory for each of them. They were tracked by considering the optimum residence time of the water vapour in the atmosphere for each continental grid point, that is, the best Lagrangian time to match the precipitation data obtained from a reference re-analysis (ERA-Interim in this case) and the Lagrangian precipitation^{70,74,75}.

The individual increases (e) and decreases (p) of humidity were calculated as $(e - p) = m(dq/dt)$. The vertical integration of these individual ($e - p$) values over each gridded area, from the surface to the top of the atmosphere, provided an estimation of the surface freshwater flux ($E - P$), where E is the evaporation and P the precipitation rate per unit area. Values over zero indicate the prevalence of evaporation in the column, whereas negative values indicate moisture loss, which normally occurs by condensation and precipitation, so it was considered as a contribution to precipitation^{25,76}. Hence, Nieto and Gimeno⁷⁰ computed those values of $(E - P) < 0$ over each grid point over the continents, which are considered as contributions to precipitation, for those air parcels with oceanic and terrestrial origin, respectively, being the both components of the total Lagrangian precipitation. The moduli of their final values were used for practical purposes.

To analyse the role of the oceanic and terrestrial moisture sources in drought events, we calculated analogous standardized indices to the SPI for every grid point using both the oceanic and terrestrial contributions to precipitation separately. Those standardized indices were denoted as SPIc.

Our approach only takes values in regions and times where the evaporation minus precipitation ($E - P$) balance is negative to define precipitation, so the dataset used mainly shows the precipitation-deficit drought, although evaporation could be relevant for drought intensification under some conditions^{77,78}. Nevertheless, the main role of precipitation on drought development and intensification is indisputable. Evapotranspiration could have a role on short time scales of precipitation deficits (for example, 1 month SPI). However, when moving to longer time scales (for example, 3 month SPI), which are representative of cumulative precipitation deficits, necessary to trigger a drought event, precipitation is the main variable controlling drought variability. Even using the atmospheric evaporative demand instead of evapotranspiration, precipitation is the main variable controlling variability of drought indices⁷⁹. It is also important to warn on the use of $(P - E)$ to assess drought severity. This is a metric that is widely used to assess changes in the water availability for long periods (from annual to decadal) and it has shown changes for the long term⁸⁰. Nevertheless, for the assessment of short-term droughts, the use of $(P - E)$ as a metric of drought severity is highly problematic, particularly during the dry season, in which E can be limited by the soil water availability, which can be determined by the precipitation over a long period. If E is suppressed given low soil moisture, this may produce situations in which under drought conditions, short time scales of $(P - E)$ may provide positive values (indicative of humid conditions), given reduced E . This was illustrated with the extreme drought that affected southwestern Europe and North Africa in 2005, in which drought severity was not identified using $(P - E)$ at short time scale⁸¹. For these reasons (and the existing uncertainties for a reliable estimation of E , including the important role of land cover changes), we consider it better to constrain our analysis to a drought metric based on precipitation, which is less uncertain, widely used for drought monitoring and early warning, and recommended by the World Meteorological Organization as the reference metric for drought quantification⁸².

As the moisture transport data is based on the ERA-Interim, in a first approximation, the uncertainties of estimating moisture transport

are those derived from the re-analysis uncertainties. For moisture transport estimation, uncertainties are mainly those linked to the correct estimation of atmospheric circulation and of the water vapour content. Owing to its construction process, based on a circulation model, one of the strong points of the re-analysis is the good reproduction of the large-scale general circulation of the atmosphere, so large uncertainties cannot be expected in this sense. Those linked to moisture content may be greater. In a very recent comparison between daily re-analysis data with the new Total Column Water Vapour Data Record (v2)—developed by the European Space Agency in coordination with the Satellite Application Facility on Climate Monitoring—Eiras-Barca et al.⁸³ showed low bias in most oceanic and continental areas, being generally less than $\pm 2 \text{ kg m}^{-2}$ in the main regions where moisture transport influences precipitation (regions of occurrence of ARs, LLJs and TCs). The temporal correlations between the re-analysis data and that new data record were above 0.8 in most areas of the world, finding the highest discrepancies in the main tropical rainforest regions.

Calculation of the contribution to precipitation from major moisture sources

Following the same methodology, we determined the individual moisture contributions to precipitation over the continents from 11 major climatological oceanic moisture sources²⁰ and two key terrestrial sources: the Amazon and Congo river basins^{84,85}, for the 1980–2018 period. In these regional forward experiments, the set of particles over each moisture source was selected.

As was done for the oceanic and terrestrial standardized indices, to analyse the role of the major moisture sources in drought events, we calculated analogous indices to the SPI for every grid point using their individual moisture contribution to precipitation. That is, we obtained the SPIC values corresponding to the contribution to precipitation from the major individual moisture sources. To analyse the three hotspot regions (CENA, SESA and EEur), the monthly MSWEP and each moisture source contribution series for the 1980–2018 period were spatially averaged over each studied region before obtaining the standardized indices.

The approach has some limitations linked to the definition of moisture source regions. Our analysis is based on a set of geographically fixed sources, namely all ocean versus all land in a first approximation and the 13 most important source regions at a global level estimated by climatological values (as revealed by the secular paper, Gimeno et al.²⁰). Therefore, it does not allow to analyse changes in the positions of the sources, although it permits changes in the intensity of moisture transport from the source to any potential sink. This change in transport can be due to either a change in evaporation from the source, a change in the circulation from source to sink, or in both. Obviously, a given sink region can have specific source regions, which can vary both in position and intensity in current and future climates. But even analysing the specific sources of a given sink region, the use of source regions of variable extension over time does not allow the approximation used in this study, based on the probability of drought occurrence given a moisture source contribution deficit, since this requires the same source extension conditions. That is why the factor ‘change in the position of the source’ is not included in this study and the climatological positions were taken as a basis. However, and for specific target regions, other non-probabilistic approximations can be used based on extension and intensity anomalies of the source regions for drought events, widely used in previous studies (for example, the catalogue by Drumond et al.²¹ for the Intergovernmental Panel on Climate Change reference regions).

Statistical method I: estimation of the conditional probability of drought occurrence given an equivalent moisture source contribution deficit

In this study, we relied on techniques from the copula theory⁸⁶ to estimate the probability of drought occurrence for a given moisture source

contribution deficit. It is increasingly popular to model the dependence structure of a pair of variables by fitting a copula model, particularly in hydroclimatic applications⁸⁷. Copulas offer a versatile framework for estimating conditional probabilities, as they enable the generation of synthetic data that preserves the observed dependence structure between the variables. It is a flexible methodology, as it is possible to choose a copula function that closely matches the observed dependence pattern. Whether relationships are linear, non-linear, symmetric or asymmetric, copula models can capture them effectively. Copulas excel in modelling tail dependence, which is crucial when studying extreme events such as droughts^{88–90}. Although other statistical methods have been used in the context of compound extreme events, such as event coincidence analysis⁹¹, multi-type point processes⁹² or counting the simultaneous/consequential occurrences of multiple extremes⁹³, the singular properties of copulas permit a complete understanding of the dependence structure of the variables⁹⁰ and that is the reason why we opted for this methodology in this study.

We followed the semiparametric approach for model fitting by obtaining uniformly transformed values of the original variables (known as pseudo-observations) and applying the maximum likelihood estimation to obtain estimates of the copula parameters⁹⁴. U_{SPI} and U_{SPIC} denoted the variables on a uniform scale. For each grid point, copula models were fitted to model the dependence structure of each $(U_{\text{SPI}}, U_{\text{SPIC}})$ pair for each moisture source contribution. For the 1 month temporal scale, all observations (monthly values) were used for model fitting. However, for the 3 month scale, only observations corresponding to March, June, September and December were considered, as they are the representative values of the corresponding seasons, that is, January–March, April–June, July–September and October–December, respectively.

We used R software⁹⁵, namely, the R package VineCopula⁹⁶. Six different types of parametric copulas were used—Gaussian, Student t , Clayton, Gumbel, Frank and Joe copulas; their expressions can be found in Czado⁹⁷. Using these copula models, it becomes possible to flexibly represent the dependence structure of the studied pair of variables. They provide a wide array of different radial asymmetry or symmetry shapes and tail dependence behaviour. Among the asymmetric models, the Clayton copula is used to model dependence in the lower tail, while the Gumbel and Joe can model upper tail dependence. Regarding the symmetric ones, the Gaussian and Frank copulas do not exhibit tail dependence, while the Student t copula can capture both lower and upper tail dependence. The independence copula (product copula) was also used, which corresponds to the case of both variables being independent.

Among the fitted copula models, the one with the lowest Akaike information criterion value was selected⁹⁸. The statistical test by Huang and Prokhorov⁹⁹ based on White’s¹⁰⁰ information matrix equality was applied to test the null hypothesis that the selected parametric copula model fits well to the data. Using the selected fitted copula model, we obtained 100,000 simulated values for the variables on a uniform scale. The large sample size allowed the estimation of the probability of the SPI being lower than its fifth percentile (approximately -1.64), conditional on the SPIC being lower than its corresponding fifth percentile (approximately -1.64), as follows:

1. Among the 100,000 simulated values of $(U_{\text{SPI}}, U_{\text{SPIC}})$, we selected the bivariate observations such that $U_{\text{SPIC}} \leq u_{\text{SPIC},5\%}$.
2. We constructed the empirical cumulative distribution function of U_{SPI} conditional on $U_{\text{SPIC}} \leq u_{\text{SPIC},5\%}$ and denoted this as $\hat{F}_{U_{\text{SPI}}|U_{\text{SPIC}} \leq u_{\text{SPIC},5\%}}$.
3. We computed $\hat{F}_{U_{\text{SPI}}|U_{\text{SPIC}} \leq u_{\text{SPIC},5\%}}(u_{\text{SPI},5\%})$, which is an estimate of $P(U_{\text{SPI}} \leq u_{\text{SPI},5\%} | U_{\text{SPIC}} \leq u_{\text{SPIC},5\%})$

$$\sim P(\text{SPI} \leq -1.64 | \text{SPIC} \leq -1.64),$$

where $u_{\text{SPI},5\%}$ and $u_{\text{SPIC},5\%}$ are the fifth percentile values of the uniformly transformed values for SPI and SPIC, respectively.

We used the same threshold (in standardized units) for both the SPI and SPIc when estimating the desired conditional probability (that is, we based our analysis on an ‘equivalent moisture deficit’) because our aim was to analyse droughts and moisture source contribution deficits defined under the same conditions.

Statistical method II: estimation of the conditional probability of drought occurrence given an observed value of moisture source contribution deficit

To estimate the conditional probability of drought occurrence given an observed value of moisture source contribution deficit for the three selected regions, the method was the same as that previously discussed in terms of model fitting. However, in this case, the 100,000 simulations were obtained from the conditional distribution function of SPI given an observed value of SPIc. That is, for an observed value of SPIc (let it be denoted as $SPIc_{obs}$, and let $u_{SPIc_{obs}}$ be the uniform-transformed value), the method is as follows:

1. We used 100,000 simulated values of $U_{SPI}|U_{SPIc} = u_{SPIc_{obs}}$ to construct its empirical cumulative distribution function, denoted as $F_{U_{SPI}|U_{SPIc} = u_{SPIc_{obs}}}$.
2. We computed $F_{U_{SPI}|U_{SPIc} = u_{SPIc_{obs}}}(u_{SPI,5\%})$, which is an estimate of $P(U_{SPI} \leq u_{SPI,5\%} | U_{SPIc} = u_{SPIc_{obs}})$

$$\sim P(SPI \leq -1.64 | SPIc = SPIc_{obs}),$$

where $u_{SPI,5\%}$ is the fifth percentile value of the uniformly transformed values for SPI.

Uncertainties in the probability estimation were assessed using a repeated sampling procedure adapted from Ribeiro et al.¹⁰¹, which enabled us to construct confidence intervals for the conditional probabilities. The procedure performed was the following: once the copula model was selected by means of the Akaike information criterion, we obtained a sample of 1,000 values for each conditional probability. Using that sample, we computed the 2.5% and 97.5% percentiles, corresponding to the lower and upper bounds of the 95% confidence interval for each conditional probability, respectively. Each of the 1,000 values of the sample was obtained by using n simulated values of $U_{SPI}|U_{SPIc} = u_{SPIc_{obs}}$, with n being the number of observations.

Reporting summary

Further information on research design is available in the Nature Portfolio Reporting Summary linked to this article.

Data availability

European Centre for Medium-Range Weather Forecasts Re-analysis dataset used to run FLEXPART and to calculate trajectories should be downloaded through the routine script available at <https://www.flexpart.eu/downloads>. Precipitation data used to calculate drought indices are taken from MSWEP, publicly available for download via <https://www.gloh2o.org/mswep/>.

Code availability

The FLEXPART model used to calculate trajectories is publicly available and can be downloaded from <https://www.flexpart.eu/wiki/FpRoadmap>. TROVA software used to calculate the contribution of the moisture sources is publicly available and can be downloaded from <https://github.com/ElsevierSoftwareX/SOFTX-D-22-00100>. For the calculation of the Standardized Precipitation Index (SPI) and the contribution indices obtained in an analogous way to SPI, the R package SPEI was used (available at <https://cran.r-project.org/web/packages/SPEI/index.html>). The conditional probability estimation was performed using the R package VineCopula (available at <https://cran.r-project.org/web/packages/VineCopula/index.html>).

References

1. WMO Atlas of Mortality and Economic Losses from Weather, Climate and Water Extremes (1970–2019) (World Meteorological Organization, 2021).
2. Smith, A. B. & Matthews, J. L. Quantifying uncertainty and variable sensitivity within the US billion-dollar weather and climate disaster cost estimates. *Nat. Hazards* **77**, 1829–1851 (2015).
3. Crausbay, S. D. et al. Defining ecological drought for the twenty-first century. *Bull. Am. Meteorol. Soc.* **98**, 2543–2550 (2017).
4. Douville, H. et al. in *Climate Change 2021: The Physical Science Basis* (eds Masson-Delmotte, V. et al.) 1055–1210 (Cambridge University Press, 2021).
5. Seneviratne, S. I. et al. in *Climate Change 2021: The Physical Science Basis* (eds Masson-Delmotte, V. et al.) 1513–1766 (Cambridge University Press, 2021).
6. Ault, T. R. On the essentials of drought in a changing climate. *Science* **368**, 256–260 (2020).
7. AghaKouchak, A., Feldman, D., Hoerling, M., Huxman, T. & Lund, J. Water and climate: recognize anthropogenic drought. *Nature* **524**, 409–411 (2015).
8. Van Loon, A. F. et al. Drought in the Anthropocene. *Nat. Geosci.* **9**, 89–91 (2016).
9. Dai, A., Zhao, T. & Chen, J. Climate change and drought: a precipitation and evaporation perspective. *Curr. Clim. Change Rep.* **4**, 301–312 (2018).
10. Schubert, S. D. et al. Global meteorological drought: a synthesis of current understanding with a focus on SST drivers of precipitation deficits. *J. Clim.* **29**, 3989–4019 (2016).
11. Kunkel, K. E., Stevens, S. E., Stevens, L. E. & Karl, T. R. Observed climatological relationships of extreme daily precipitation events with precipitable water and vertical velocity in the contiguous United States. *Geophys. Res. Lett.* **47**, e2019GL086721 (2020).
12. Hagos, S. M. et al. The relationship between precipitation and precipitable water in CMIP6 simulations and implications for tropical climatology and change. *J. Clim.* **34**, 1587–1600 (2021).
13. Trenberth, K. E., Branstator, G. W. & Arkin, P. A. Origins of the 1988 North American drought. *Science* **242**, 1640–1645 (1988).
14. Trenberth, K. E., Dai, A., Rasmussen, R. M. & Parsons, D. B. The changing character of precipitation. *Bull. Am. Meteorol. Soc.* **84**, 1205–1218 (2003).
15. Gimeno, L. et al. Major mechanisms of atmospheric moisture transport and their role in extreme precipitation events. *Annu. Rev. Environ. Resources* **41**, 117–141 (2016).
16. Eltahir, E. A. B. & Bras, R. L. Precipitation recycling. *Rev. Geophys.* **34**, 367–378 (1996).
17. van der Ent, R. J., Savenije, H. H., Schaeffli, B., & Steele-Dunne, S. C. Origin and fate of atmospheric moisture over continents. *Water Resour. Res.* <https://doi.org/10.1029/2010WR009127> (2010).
18. Gimeno, L. et al. Oceanic and terrestrial sources of continental precipitation. *Rev. Geophys.* **50**, RG4003 (2012).
19. Gimeno, L., Nieto R., & Sorí R. The growing importance of oceanic moisture sources for continental precipitation. *NPJ Clim Atmos. Sci.* <https://doi.org/10.1038/s41612-020-00133-y> (2020).
20. Gimeno, L., Drumond A., Nieto R., Trigo R. M., & Stohl A. On the origin of continental precipitation. *Geophys. Res. Lett.* <https://doi.org/10.1029/2010GL043712> (2010).
21. Drumond, A., Stojanovic, M., Nieto, R., Vicente-Serrano, S. M. & Gimeno, L. Linking anomalous moisture transport and drought episodes in the IPCC reference regions. *Bull. Amer. Meteor. Soc.* **100**, 1481–1498 (2019).
22. Shen, Z. et al. Drying in the low-latitude Atlantic Ocean contributed to terrestrial water storage depletion across Eurasia. *Nat. Commun.* **13**, 1849 (2022).

23. Rathore, S., Bindoff, N. L., Ummenhofer, C. C., Phillips, H. E. & Feng, M. Near-surface salinity reveals the oceanic sources of moisture for Australian precipitation through atmospheric moisture transport. *J. Clim.* **33**, 6707–6730 (2020).
24. Vázquez, M., Nieto, R., Liberato, M. L. R. & Gimeno, L. Atmospheric moisture sources associated with extreme precipitation during the peak precipitation month. *Weather Clim. Extrem.* **30**, 100289 (2020).
25. Stohl, A. & James, P. A Lagrangian analysis of the atmospheric branch of the global water cycle. Part II: moisture transports between Earth's ocean basins and river catchments. *J. Hydrometeorol.* **6**, 961–984 (2005).
26. Tuinenburg, O. A., Theeuwes, J. J. E. & Staal, A. High-resolution global atmospheric moisture connections from evaporation to precipitation. *Earth Syst. Sci. Data* **12**, 3177–3188 (2020).
27. Dey, D., Aldama Campino, A. & Döös, K. Atmospheric water transport connectivity within and between ocean basins and land. *Hydrol. Earth Syst. Sci.* **27**, 481–493 (2023).
28. Herrera-Estrada, J. E., Satoh, Y. & Sheffield, J. Spatiotemporal dynamics of global drought. *Geophys. Res. Lett.* **44**, 2254–2263 (2017).
29. Dorigo, W., et al. Closing the water cycle from observations across scales: where do we stand? *Bull. Am. Meteorol. Soc.* <https://doi.org/10.1175/BAMS-D-19-0316.1> (2021).
30. Oki, T. & Kanae, S. Global hydrological cycles and world water resources. *Science* **313**, 1068–1072 (2006).
31. Gimeno-Sotelo, L. & Gimeno, L. Where does the link between atmospheric moisture transport and extreme precipitation matter? *Weather Clim. Extrem.* **39**, 100536 (2023).
32. Lavers, D. A. & Villarini, G. The contribution of atmospheric rivers to precipitation in Europe and the United States. *J. Hydrol.* **522**, 382–390 (2015).
33. Khouakhi, A., Villarini, G. & Vecchi, G. A. Contribution of tropical cyclones to rainfall at the global scale. *J. Clim.* **30**, 359–372 (2017).
34. Jones, C. Recent changes in the South America low-level jet. *NPJ Clim. Atmos. Sci.* **2**, 20 (2019).
35. Schumacher, D. L., Keune, J., Dirmeyer, P. & Miralles, D. G. Drought self-propagation in drylands due to land–atmosphere feedbacks. *Nat. Geosci.* **15**, 262–268 (2022).
36. Pan, S. et al. Responses of global terrestrial evapotranspiration to climate change and increasing atmospheric CO₂ in the 21st century. *Earths Future* **3**, 15–35 (2015).
37. Payne, A. E. et al. Responses and impacts of atmospheric rivers to climate change. *Nat. Rev. Earth Environ.* **1**, 143–157 (2020).
38. Torres-Alvarez, J. A. et al. Future projections in the climatology of global low-level jets from CORDEX-CORE simulations. *Clim. Dyn.* **57**, 1551–1569 (2021).
39. Knutson, T. et al. Tropical cyclones and climate change assessment: part II: projected response to anthropogenic warming. *Bull. Am. Meteorol. Soc.* **101**, E303–E322 (2020).
40. Ropelewski, C. F. & Halpert, M. S. Global and regional scale precipitation patterns associated with the El Niño/Southern Oscillation. *Mon. Wea. Rev.* **115**, 1606–1626 (1987).
41. Hurrell, J. Decadal trends in the North-Atlantic oscillation: regional temperatures and precipitation. *Science* **269**, 676–679 (1995).
42. Byrne, M. P. & O’Gorman, P. A. Trends in continental temperature and humidity directly linked to ocean warming. *Proc. Natl Acad. Sci. USA* **115**, 4863–4868 (2018).
43. Wainwright, C. M., Allan, R. P. & Black, E. Consistent trends in dry spell length in recent observations and future projections. *Geophys. Res. Lett.* **49**, e2021GL097231 (2022).
44. Hao, Z., Singh, V. P. & Xia, Y. Seasonal drought prediction: advances, challenges, and future prospects. *Rev. Geophys.* **56**, 108–141 (2018).
45. Doblaz-Reyes, F. J., García-Serrano, J., Lienert, F., Biescas, A. P. & Rodrigues, L. R. L. Seasonal climate predictability and forecasting: status and prospects. *WIREs Clim. Change* **4**, 245–268 (2013).
46. Yuan, X. & Wood, E. F. Multimodel seasonal forecasting of global drought onset. *Geophys. Res. Lett.* **40**, 4900–4905 (2013).
47. Hoerling, M. et al. Causes and predictability of the 2012 Great Plains drought. *Bull. Am. Meteor. Soc.* <https://doi.org/10.1175/BAMS-D-13-00055.1> (2014).
48. Lavers, D. A., Waliser, D. E., Ralph, F. M. & Dettinger, M. D. Predictability of horizontal water vapor transport relative to precipitation: enhancing situational awareness for forecasting western U.S. extreme precipitation and flooding. *Geophys. Res. Lett.* **43**, 2275–2282 (2016).
49. Lavers, D. A., Pappenberger, F. & Zsoter, E. Extending medium-range predictability of extreme hydrological events in Europe. *Nat. Commun.* **5**, 5382 (2014).
50. Gvoždíková, B. & Müller, M. Predictability of moisture flux anomalies indicating central European extreme precipitation events. *Q. J. R. Meteorol. Soc.* **147**, 3335–3348 (2021).
51. Wang, S. & Yuan, X. Extending seasonal predictability of Yangtze River summer floods. *Hydrol. Earth Syst. Sci.* **22**, 4201–4211 (2018).
52. Gao, S., Liu, P. & Lall, U. Seasonal precipitation predictability for the northern hemisphere using concurrent and pre-season atmospheric water vapor transport and sea surface temperature. *J. Hydrometeorol.* **22**, 183–199 (2021).
53. Allan, R. P. et al. Advances in understanding large-scale responses of the water cycle to climate change. *Ann. NY Acad. Sci.* **1472**, 49–75 (2020).
54. Mamalakis, A. et al. Zonally contrasting shifts of the tropical rain belt in response to climate change. *Nat. Clim. Chang.* **11**, 143–151 (2021).
55. Allan, R. P., Willett, K. M., John, V. O. & Trent, T. Global changes in water vapor 1979–2020. *J. Geophys. Res. Atmos.* **127**, e2022JD036728 (2022).
56. Pendergrass, A. G. et al. Flash droughts present a new challenge for subseasonal-to-seasonal prediction. *Nat. Clim. Change* **10**, 191–199 (2020).
57. Tan, X. et al. Increasing global precipitation whiplash due to anthropogenic greenhouse gas emissions. *Nat. Commun.* **14**, 2796 (2023).
58. McKee, T. B., Doesken, N. J., & Kleist, J. The relationship of drought frequency and duration to time scales. In *Proceedings of the 8th Conference on Applied Climatology* Vol. 17, 179–183 (1993).
59. Vicente-Serrano, S. M., Beguería, S. & López-Moreno, J. I. A multiscalar drought index sensitive to global warming: the Standardized Precipitation Evapotranspiration Index. *J. Climate* **23**, 1696–1718 (2010).
60. Hobbins, M. T. et al. The evaporative demand drought index. Part I: linking drought evolution to variations in evaporative demand. *J. Hydrometeorol.* **17**, 1745–1761 (2016).
61. World Meteorological Organization. *Standardized Precipitation Index User Guide* <https://library.wmo.int/records/item/39629-standardized-precipitation-index-user-guide> (2012).
62. Barker, L. J., Hannaford, J., Chiverton, A. & Svensson, C. From meteorological to hydrological drought using standardised indicators. *Hydrol. Earth Syst. Sci.* **20**, 2483–2505 (2016).
63. Peña-Gallardo, M. et al. Complex influences of meteorological drought time-scales on hydrological droughts in natural basins of the contiguous United States. *J. Hydrol.* **568**, 611–625 (2019).
64. Beck, H. E. et al. MSWEP V2 global 3-hourly 0.1 precipitation: methodology and quantitative assessment. *Bull. Am. Meteorol. Soc.* **100**, 473–500 (2019).

65. Awange, J. L., Hu, K. X. & Khaki, M. The newly merged satellite remotely sensed, gauge and reanalysis-based Multi-Source Weighted-Ensemble Precipitation: evaluation over Australia and Africa (1981–2016). *Sci. Total Environ.* **670**, 448–465 (2019).
66. Mekonnen, K. et al. Accuracy of satellite and reanalysis rainfall estimates over Africa: a multi-scale assessment of eight products for continental applications. *J. Hydrol. Reg. Stud.* **49**, 101514 (2023).
67. Hersbach, H. et al. The ERA5 global reanalysis. *Q. J. R. Meteorol. Soc.* **146**, 1999–2049 (2020).
68. Lavers, D. A., Simmons, A., Vamborg, F. & Rodwell, M. J. An evaluation of ERA5 precipitation for climate monitoring. *Q. J. R. Meteorol. Soc.* **148**, 3124–3137 (2022).
69. Nieto, R. & Gimeno, L. A database of optimal integration times for Lagrangian studies of atmospheric moisture sources and sinks. *Sci. Data* **6**, 59 (2019).
70. Nieto, R. & Gimeno, L. Addendum: a database of optimal integration times for Lagrangian studies of atmospheric moisture sources and sinks. *Sci. Data* **8**, 130 (2021).
71. Stohl, A., Forster, C., Frank, A., Seibert, P. & Wotawa, G. The Lagrangian particle dispersion model FLEXPART version 6.2. *Atmos. Chem. Phys.* **5**, 2461–2474 (2005).
72. Pissot, I. et al. The Lagrangian particle dispersion model FLEXPART version 10.4. *Geosci. Model Dev.* **12**, 4955–4997 (2019).
73. Dee, D. P. et al. The ERA-Interim reanalysis: configuration and performance of the data assimilation system. *Q. J. R. Meteorol. Soc.* **137**, 553–597 (2011).
74. Nieto, R., & Gimeno, L. Optimal integration times for Lagrangian studies of atmospheric moisture sources and sinks. *Zenodo* <https://doi.org/10.5281/zenodo.1453841> (2018).
75. Gimeno, L. et al. The residence time of water vapour in the atmosphere. *Nat. Rev. Earth Environ.* **2**, 558–569 (2021).
76. Stohl, A. & James, P. A Lagrangian analysis of the atmospheric branch of the global water cycle. Part I: method description, validation, and demonstration for the August 2002 flooding in central Europe. *J. Hydrometeorol.* **5**, 656–678 (2004).
77. Teuling, A. J. et al. Evapotranspiration amplifies European summer drought. *Geophys. Res. Lett.* **40**, 2071–2075 (2013).
78. Zhao, M., A. G., Liu, Y. & Konings, A. G. Evapotranspiration frequently increases during droughts. *Nat. Clim. Change* **12**, 1024–1030 (2022).
79. Tomas-Burguera, M. et al. Global characterization of the varying responses of the standardized precipitation evapotranspiration index to atmospheric evaporative demand. *J. Geophys. Res. Atmospheres* **125**, e2020JD033017 (2020).
80. Padrón, R. S. et al. Observed changes in dry-season water availability attributed to human-induced climate change. *Nat. Geosci.* **13**, 477–481 (2020).
81. Vicente-Serrano, S. M. et al. Global drought trends and future projections. *Philos. Trans. R. Soc. Math. Phys. Eng. Sci.* <https://doi.org/10.1098/rsta.2021.0285> (2022).
82. Hayes, M., Svoboda, M., Wall, N. & Widhalm, M. The lincoln declaration on drought indices: universal meteorological drought index recommended. *Bull. Am. Meteorol. Soc.* **92**, 485–488 (2011).
83. Eiras-Barca, J. et al. Analysis of the main source regions of moisture transport events with the new ESA CCI/CM-SAF total column water vapour climate data record (v2). *Q. J. R. Meteorol. Soc.* **148**, 3244–3258 (2022).
84. Drumond, A. et al. The role of the Amazon Basin moisture in the atmospheric branch of the hydrological cycle: a Lagrangian analysis. *Hydrol. Earth Syst. Sci.* **18**, 2577–2598 (2014).
85. Sorí, R., Nieto, R., Vicente-Serrano, S. M., Drumond, A. & Gimeno, L. A Lagrangian perspective of the hydrological cycle in the Congo River basin. *Earth System Dynamics* **8**, 653–675 (2017).
86. Nelsen, R. B. *An Introduction to Copulas* (Springer, 2007).
87. Tootoonchi, F. et al. Copulas for hydroclimatic analysis: a practice-oriented overview. *Wiley Interdiscip. Rev. Water* **9**, e1579 (2022).
88. Brunner, M. I., Liechti, K. & Zappa, M. Extremeness of recent drought events in Switzerland: dependence on variable and return period choice. *Nat. Hazards Earth Syst. Sci.* **19**, 2311–2323 (2019).
89. Ribeiro, A. F., Russo, A., Gouveia, C. M. & Páscoa, P. Copula-based agricultural drought risk of rainfed cropping systems. *Agric. Water Manage.* **223**, 105689 (2019).
90. Ribeiro, A. F., Russo, A., Gouveia, C. M. & Pires, C. A. Drought-related hot summers: a joint probability analysis in the Iberian Peninsula. *Weather Clim. Extrem.* **30**, 100279 (2020).
91. Donges, J. F., Schleussner, C. F., Siegmund, J. F. & Donner, R. V. Event coincidence analysis for quantifying statistical interrelationships between event time series: on the role of flood events as triggers of epidemic outbreaks. *Eur. Phys. J. Spec. Top.* **225**, 471–487 (2016).
92. Toreti, A., Cronie, O. & Zampieri, M. Concurrent climate extremes in the key wheat producing regions of the world. *Sci. Rep.* **9**, 5493 (2019).
93. Wu, X., Hao, Z., Hao, F., Li, C., & Zhang, X. Spatial and temporal variations of compound droughts and hot extremes in China. *Atmosphere* <https://doi.org/10.3390/atmos10020095> (2019).
94. Shemyakin, A., & Kniazev, A. *Introduction to Bayesian Estimation and Copula Models of Dependence* (Wiley, 2017).
95. R Core Team. R: a language and environment for statistical computing. *R Foundation for Statistical Computing* <https://www.R-project.org/> (2022).
96. Nagler, T., et al. VineCopula: statistical inference of vine copulas, R package version 2.4.3. *R Project* <https://CRAN.R-project.org/package=VineCopula> (2021).
97. Czado, C. *Analyzing Dependent Data with Vine Copulas* (Springer, 2019).
98. Akaike, H. A new look at the statistical model identification. *IEEE Trans. Autom. Control* **19**, 716–723 (1974).
99. Huang, W. & Prokhorov, A. A goodness-of-fit test for copulas. *Econ. Rev.* **33**, 751–771 (2014).
100. White, H. Maximum likelihood estimation of misspecified models. *Econometrica* **50**, 1–25 (1982).
101. Ribeiro, A. F. S., Russo, A., Gouveia, C. M., Páscoa, P. & Zscheischler, J. Risk of crop failure due to compound dry and hot extremes estimated with nested copulas. *Biogeosciences* **17**, 4815–4830 (2020).

Acknowledgements

EPhysLab members were supported by SETESTRELO project (grant no. PID2021-122314OB-I00) funded by the Ministerio de Ciencia, Innovación y Universidades, Spain (MCIN/10.13039/501100011033), Xunta de Galicia (grant ED431C2021/44; Programa de Consolidación e Estructuración de Unidades de Investigación Competitivas (Grupos de Referencia Competitiva), Consellería de Cultura, Educación e Universidade) and ‘ERDF A way of making Europe’. L.G.-S. was supported by a ‘Ministerio de Ciencia, Innovación y Universidades’ PhD grant (reference: PRE2022-101497) and R.S. by a ‘Spanish Ministry Ramon y Cajal’ grant. We thank M. Vázquez for providing necessary data for this study. In addition, this work was possible because of the computing resources and technical support provided by the Centro de Supercomputación de Galicia (CESGA). This study was also supported by the ‘Unidad Asociada CSIC-Universidade de Vigo: Grupo de Física de la Atmósfera y del Océano’. This publication is

part of the ESMORGA I+D+i project (TED2021-129152B-C43), funded by the MICIU/AEI/10.13039/501100011033 and the European Union NextGenerationEU/PRTR.

Author contributions

L.G.-S. designed the experiments and contributed to data analysis and the writing of the paper. R.S. performed the Lagrangian analysis and contributed to the writing of the paper. R.N. contributed to the creation of the final figures and the writing of the paper. S.M.V.-S. contributed to the discussion of results. L.G. conceived the idea of the study and contributed to the writing of the paper. All authors contributed to the review and editing of the paper.

Competing interests

The authors declare no competing interests.

Additional information

Supplementary information The online version contains supplementary material available at <https://doi.org/10.1038/s44221-023-00192-4>.

Correspondence and requests for materials should be addressed to Luis Gimeno.

Peer review information *Nature Water* thanks Richard Allan, Xuezhi Tan and Ricardo Trigo for their contribution to the peer review of this work.

Reprints and permissions information is available at www.nature.com/reprints.

Publisher's note Springer Nature remains neutral with regard to jurisdictional claims in published maps and institutional affiliations.

Open Access This article is licensed under a Creative Commons Attribution 4.0 International License, which permits use, sharing, adaptation, distribution and reproduction in any medium or format, as long as you give appropriate credit to the original author(s) and the source, provide a link to the Creative Commons license, and indicate if changes were made. The images or other third party material in this article are included in the article's Creative Commons license, unless indicated otherwise in a credit line to the material. If material is not included in the article's Creative Commons license and your intended use is not permitted by statutory regulation or exceeds the permitted use, you will need to obtain permission directly from the copyright holder. To view a copy of this license, visit <http://creativecommons.org/licenses/by/4.0/>.

© The Author(s) 2024, corrected publication 2025

Reporting Summary

Nature Portfolio wishes to improve the reproducibility of the work that we publish. This form provides structure for consistency and transparency in reporting. For further information on Nature Portfolio policies, see our [Editorial Policies](#) and the [Editorial Policy Checklist](#).

Statistics

For all statistical analyses, confirm that the following items are present in the figure legend, table legend, main text, or Methods section.

- | n/a | Confirmed |
|-------------------------------------|--|
| <input type="checkbox"/> | <input checked="" type="checkbox"/> The exact sample size (n) for each experimental group/condition, given as a discrete number and unit of measurement |
| <input checked="" type="checkbox"/> | <input type="checkbox"/> A statement on whether measurements were taken from distinct samples or whether the same sample was measured repeatedly |
| <input type="checkbox"/> | <input checked="" type="checkbox"/> The statistical test(s) used AND whether they are one- or two-sided
<i>Only common tests should be described solely by name; describe more complex techniques in the Methods section.</i> |
| <input type="checkbox"/> | <input checked="" type="checkbox"/> A description of all covariates tested |
| <input checked="" type="checkbox"/> | <input type="checkbox"/> A description of any assumptions or corrections, such as tests of normality and adjustment for multiple comparisons |
| <input type="checkbox"/> | <input checked="" type="checkbox"/> A full description of the statistical parameters including central tendency (e.g. means) or other basic estimates (e.g. regression coefficient) AND variation (e.g. standard deviation) or associated estimates of uncertainty (e.g. confidence intervals) |
| <input type="checkbox"/> | <input checked="" type="checkbox"/> For null hypothesis testing, the test statistic (e.g. F , t , r) with confidence intervals, effect sizes, degrees of freedom and P value noted
<i>Give P values as exact values whenever suitable.</i> |
| <input checked="" type="checkbox"/> | <input type="checkbox"/> For Bayesian analysis, information on the choice of priors and Markov chain Monte Carlo settings |
| <input checked="" type="checkbox"/> | <input type="checkbox"/> For hierarchical and complex designs, identification of the appropriate level for tests and full reporting of outcomes |
| <input type="checkbox"/> | <input checked="" type="checkbox"/> Estimates of effect sizes (e.g. Cohen's d , Pearson's r), indicating how they were calculated |

Our web collection on [statistics for biologists](#) contains articles on many of the points above.

Software and code

Policy information about [availability of computer code](#)

Data collection

The FLEXPART model used to calculate trajectories is publicly available and can be downloaded from <https://www.flexpart.eu/wiki/FpRoadmap>.
TROVA software used to calculate the contribution of the moisture sources is publicly available and can be downloaded from <https://github.com/ElsevierSoftwareX/SOFTX-D-22-00100>.

Data analysis

For the calculation of the Standardised Precipitation Index (SPI) and the contribution indices obtained in an analogous way to SPI, the R package SPEI was used (available at <https://cran.r-project.org/web/packages/SPEI/index.html>). The conditional probability estimation was performed using the R package VineCopula (available at <https://cran.r-project.org/web/packages/VineCopula/index.html>).

For manuscripts utilizing custom algorithms or software that are central to the research but not yet described in published literature, software must be made available to editors and reviewers. We strongly encourage code deposition in a community repository (e.g. GitHub). See the Nature Portfolio [guidelines for submitting code & software](#) for further information.

Data

Policy information about [availability of data](#)

All manuscripts must include a [data availability statement](#). This statement should provide the following information, where applicable:

- Accession codes, unique identifiers, or web links for publicly available datasets
- A description of any restrictions on data availability
- For clinical datasets or third party data, please ensure that the statement adheres to our [policy](#)

European Centre for Medium-Range Weather Forecasts Reanalysis dataset used to run FLEXPART and to calculate trajectories should be downloaded through the routine script available at <https://www.flexpart.eu/downloads>

Precipitation data used to calculate drought indices are taken from MSWEP, publicly available for download via <https://www.gloh2o.org/mswep/>

Research involving human participants, their data, or biological material

Policy information about studies with [human participants or human data](#). See also policy information about [sex, gender \(identity/presentation\), and sexual orientation](#) and [race, ethnicity and racism](#).

Reporting on sex and gender

Use the terms sex (biological attribute) and gender (shaped by social and cultural circumstances) carefully in order to avoid confusing both terms. Indicate if findings apply to only one sex or gender; describe whether sex and gender were considered in study design; whether sex and/or gender was determined based on self-reporting or assigned and methods used. Provide in the source data disaggregated sex and gender data, where this information has been collected, and if consent has been obtained for sharing of individual-level data; provide overall numbers in this Reporting Summary. Please state if this information has not been collected. Report sex- and gender-based analyses where performed, justify reasons for lack of sex- and gender-based analysis.

Reporting on race, ethnicity, or other socially relevant groupings

Please specify the socially constructed or socially relevant categorization variable(s) used in your manuscript and explain why they were used. Please note that such variables should not be used as proxies for other socially constructed/relevant variables (for example, race or ethnicity should not be used as a proxy for socioeconomic status). Provide clear definitions of the relevant terms used, how they were provided (by the participants/respondents, the researchers, or third parties), and the method(s) used to classify people into the different categories (e.g. self-report, census or administrative data, social media data, etc.) Please provide details about how you controlled for confounding variables in your analyses.

Population characteristics

Describe the covariate-relevant population characteristics of the human research participants (e.g. age, genotypic information, past and current diagnosis and treatment categories). If you filled out the behavioural & social sciences study design questions and have nothing to add here, write "See above."

Recruitment

Describe how participants were recruited. Outline any potential self-selection bias or other biases that may be present and how these are likely to impact results.

Ethics oversight

Identify the organization(s) that approved the study protocol.

Note that full information on the approval of the study protocol must also be provided in the manuscript.

Field-specific reporting

Please select the one below that is the best fit for your research. If you are not sure, read the appropriate sections before making your selection.

Life sciences Behavioural & social sciences Ecological, evolutionary & environmental sciences

For a reference copy of the document with all sections, see nature.com/documents/nr-reporting-summary-flat.pdf

Ecological, evolutionary & environmental sciences study design

All studies must disclose on these points even when the disclosure is negative.

Study description

Research sample

Sampling strategy

Data collection

Timing and spatial scale

Data exclusions	No data exclusion
Reproducibility	Data and software is freely available so the study has full reproducibility
Randomization	There is no randomization
Blinding	There is no blinding

Did the study involve field work? Yes No

Reporting for specific materials, systems and methods

We require information from authors about some types of materials, experimental systems and methods used in many studies. Here, indicate whether each material, system or method listed is relevant to your study. If you are not sure if a list item applies to your research, read the appropriate section before selecting a response.

Materials & experimental systems

n/a	Included in the study
<input checked="" type="checkbox"/>	<input type="checkbox"/> Antibodies
<input checked="" type="checkbox"/>	<input type="checkbox"/> Eukaryotic cell lines
<input checked="" type="checkbox"/>	<input type="checkbox"/> Palaeontology and archaeology
<input checked="" type="checkbox"/>	<input type="checkbox"/> Animals and other organisms
<input checked="" type="checkbox"/>	<input type="checkbox"/> Clinical data
<input checked="" type="checkbox"/>	<input type="checkbox"/> Dual use research of concern
<input checked="" type="checkbox"/>	<input type="checkbox"/> Plants

Methods

n/a	Included in the study
<input checked="" type="checkbox"/>	<input type="checkbox"/> ChIP-seq
<input checked="" type="checkbox"/>	<input type="checkbox"/> Flow cytometry
<input checked="" type="checkbox"/>	<input type="checkbox"/> MRI-based neuroimaging

Plants

Seed stocks	<i>Report on the source of all seed stocks or other plant material used. If applicable, state the seed stock centre and catalogue number. If plant specimens were collected from the field, describe the collection location, date and sampling procedures.</i>
Novel plant genotypes	<i>Describe the methods by which all novel plant genotypes were produced. This includes those generated by transgenic approaches, gene editing, chemical/radiation-based mutagenesis and hybridization. For transgenic lines, describe the transformation method, the number of independent lines analyzed and the generation upon which experiments were performed. For gene-edited lines, describe the editor used, the endogenous sequence targeted for editing, the targeting guide RNA sequence (if applicable) and how the editor was applied.</i>
Authentication	<i>Describe any authentication procedures for each seed stock used or novel genotype generated. Describe any experiments used to assess the effect of a mutation and, where applicable, how potential secondary effects (e.g. second site T-DNA insertions, mosaicism, off-target gene editing) were examined.</i>